Approaching conformality with the Tensor Renormalization Group method

Yannick Meurice

The University of Iowa

yannick-meurice@uiowa.edu

Work done with Yuzhi Liu, James Osborn, Judah Unmuth-Yockey (Ph. D. 2016), Zhiyuan Xie, Li-Ping Yang, and Haiyuan Zou

in part in arXiv:1507.01471

Lattice 2015, Kobe, July 15

Content of the Talk

1. Tensor Renormalization Group (TRG) formulation of the $O(2)$ model with a chemical potential
2. Comparison of particle number distributions with the worm algorithm
3. TRG calculation of the thermal entropy and entanglement entropy in the superfluid (gapless) phase
4. Fine structure of the entanglement entropy and its mirror symmetry with respect to half-filling
5. Approximate picture of weakly interacting loops with winding number one (explanation of a particle-hole symmetry without fundamental fermionic fields)
6. Numerical optimization based on particle number conservation
7. Conclusions

For details see arXiv:1507.01471

The Tensor Renormalization Group (TRG) Method

- Exact blocking (spin and gauge, PRD 88 056005)
- Applies to many lattice models: Ising model, $O(2)$ model, $O(3)$ model, Principal chiral models, Abelian and $SU(2)$ gauge theories
- Can be related to (worm) sampling methods (Prokofiev, Svistunov, Banerjee, Chandrasekharan, Gattringer ...)
- Solution of sign problems (PRD 89, 016008)
- Critical exponents (Y.M. PRB 87, 064422, Kadanoff et al. RMP 86)
- Used to design quantum simulators: $O(2)$ model with a chemical potential (PRA 90, 063603), Abelian Higgs model on optical lattices (1503.08354, Alexei Bazavov's talk, Saturday 9AM 404)
- Schwinger model: Yuya Shimizu and Yoshinobu Kuramashi, 1 flavor of Wilson fermion, arxiv 1403.0642 Phys. Rev. D 90, 014508 and 074503 (2014).
- Related method: Mari Carmen Bañuls, Krzysztof Cichy, J. Ignacio Cirac, Karl Jansen, Hana Saito, Matrix Product States for Lattice Field Theories, arXiv:1310.4118 (Lattice 2013).

2D $O(2)$ model with chemical potential μ

$$Z = \int \prod_{(x,t)} \frac{d\theta_{(x,t)}}{2\pi} e^{-S}.$$

complex action

$$\begin{aligned} S = & - \beta_{\hat{t}} \sum_{(x,t)} \cos(\theta_{(x,t+1)} - \theta_{(x,t)} - i\mu) \\ & - \beta_{\hat{x}} \sum_{(x,t)} \cos(\theta_{(x+1,t)} - \theta_{(x,t)}). \end{aligned}$$

Loop representation:

$$\begin{aligned} Z = & \sum_{\{n\}} \prod_{(x,t)} I_{n_{(x,t),\hat{x}}}(\beta_{\hat{x}}) I_{n_{(x,t),\hat{t}}}(\beta_{\hat{t}}) e^{\mu n_{(x,t),\hat{t}}} \\ & \times \delta_{n_{(x-1,t),\hat{x}} + n_{(x,t-1),\hat{t}}, n_{(x,t),\hat{x}} + n_{(x,t),\hat{t}}} . \end{aligned}$$

In all numerical calculations made here, $\beta_{\hat{x}} = \beta_{\hat{t}} = \beta$

Worm configurations

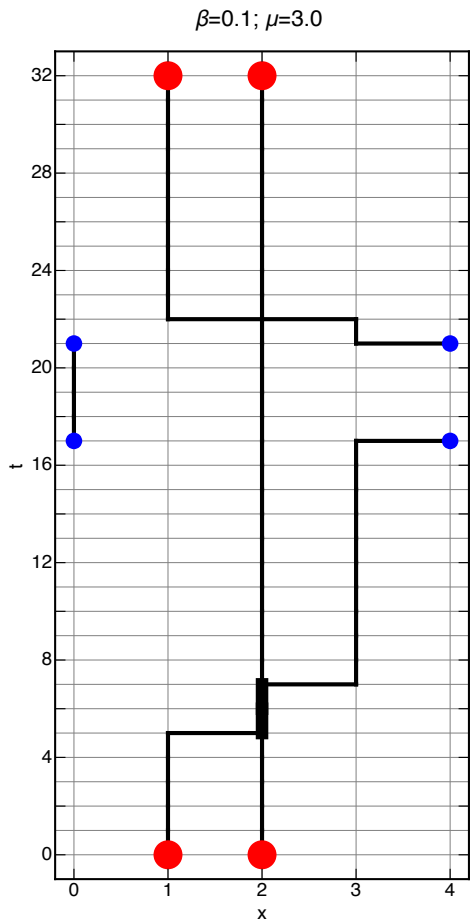

Figure: Allowed configuration of $\{n\}$ for a 4 by 32 lattice. The uncovered links on the grid have n=0, the more pronounced dark lines have $|n|$=1 and the wider lines have n=2. The dots need to be identified periodically. The time slice 5, represents a transition between $|1100\rangle$ and $|0200\rangle$.

TRG approach of the transfer matrix

The partition function can be expressed in terms of a transfer matrix:

$$Z = \mathrm{Tr}\,\mathbb{T}^{L_t} \ .$$

The matrix elements of $\mathbb{T}$ can be expressed as a product of tensors associated with the sites of a time slice (fixed t) and traced over the space indices (PhysRevA.90.063603)

$$\mathbb{T}_{(n_1,n_2,\ldots n_{L_x})(n'_1,n'_2\ldots n'_{L_x})} = \sum_{\tilde{n}_1\tilde{n}_2\ldots\tilde{n}_{L_x}} T^{(1,t)}_{\tilde{n}_{L_x}\tilde{n}_1 n_1 n'_1} T^{(2,t)}_{\tilde{n}_1\tilde{n}_2 n_2 n'_2\ldots} \cdots T^{(L_x,t)}_{\tilde{n}_{L_x-1}\tilde{n}_{L_x} n_{L_x} n'_{L_x}}$$

with

$$T^{(x,t)}_{\tilde{n}_{x-1}\tilde{n}_x n_x n'_x} = \sqrt{I_{n_x}(\beta_{\hat{t}})I_{n'_x}(\beta_{\hat{t}})I_{\tilde{n}_{x-1}}(\beta_{\hat{x}})I_{\tilde{n}_x}(\beta_{\hat{x}})\mathrm{e}^{(\mu(n_x+n'_x))}}\delta_{\tilde{n}_{x-1}+n_x,\tilde{n}_x+n'_x}$$

The Kronecker delta function reflects the existence of a conserved current, a good quantum number ("particle number").

Coarse-graining of the transfer matrix

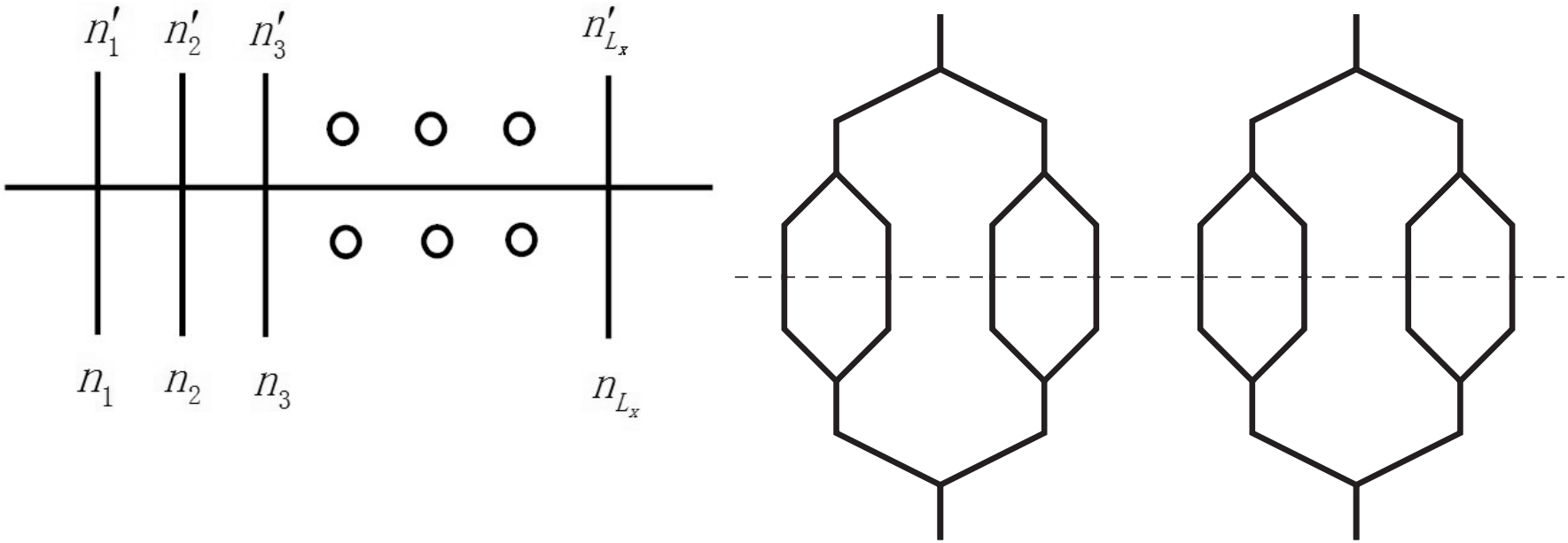

Figure: Graphical representation of the transfer matrix (left) and its successive coarse graining (right). See PRD 88 056005 and PRA 90, 063603 for explicit formulas.

Relevant region of the phase diagram

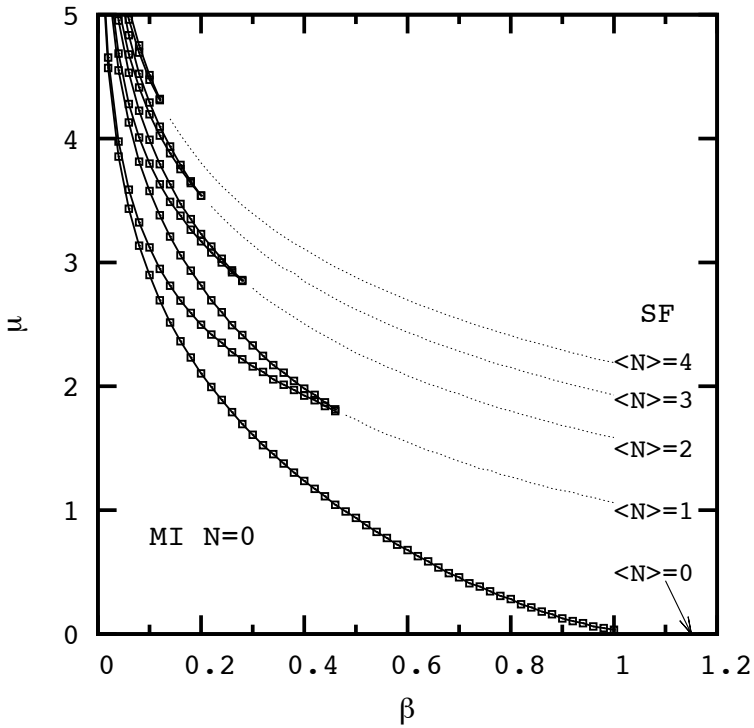

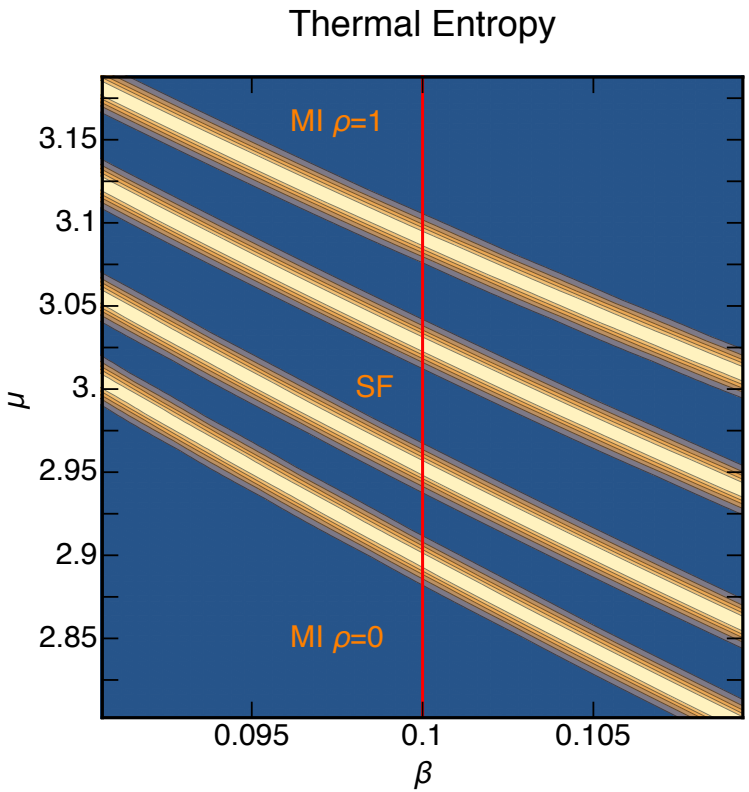

Figure: Left: Mott Insulating “tongues" ($\partial\rho/\partial\mu = 0$) immersed in the superfluid ($\partial\rho/\partial\mu \neq 0$, gapless) phase. There are KT transitions at the tips. Right: Intensity plot for the thermal entropy of the classical XY model on a 4×128 lattice in a small region of the β-μ plane. The dark (blue) regions are close to zero and the light (yellow ochre) regions peak near $\ln 2$.

Particle density calculations

The average particle number density is defined as

$$\rho = \frac{1}{L_x L_t} \frac{\partial LnZ}{\partial \mu}$$

$\partial Z/\partial\mu = L_t \mathrm{Tr}(\mathbb{T}'\mathbb{T}^{L_t-1})$, with $\mathbb{T}' = \partial\mathbb{T}/\partial\mu$ can be calculated by using the chain rule (new tensor with exact blocking formula).
A particle number $n(i)$ is associated with each eigenvalue λ_i of $\mathbb{T}$ and

$$\frac{1}{L_t}\frac{\partial \ln Z}{\partial \mu} = \frac{\sum_i \lambda_i^{L_t} n(i)}{\sum_i \lambda_i^{L_t}}.$$

Probability $P(n)$ for the particle number n:

$$P(n) = \sum_{i:n(i)=n} \lambda_i^{L_t} / \sum_i \lambda_i^{L_t}$$

These probabilities can also be calculated directly from histograms obtained with the worm algorithm (Banerjee and Chandrasekharan, PRD 81).

Comparison of the TRG and worm particle number histograms

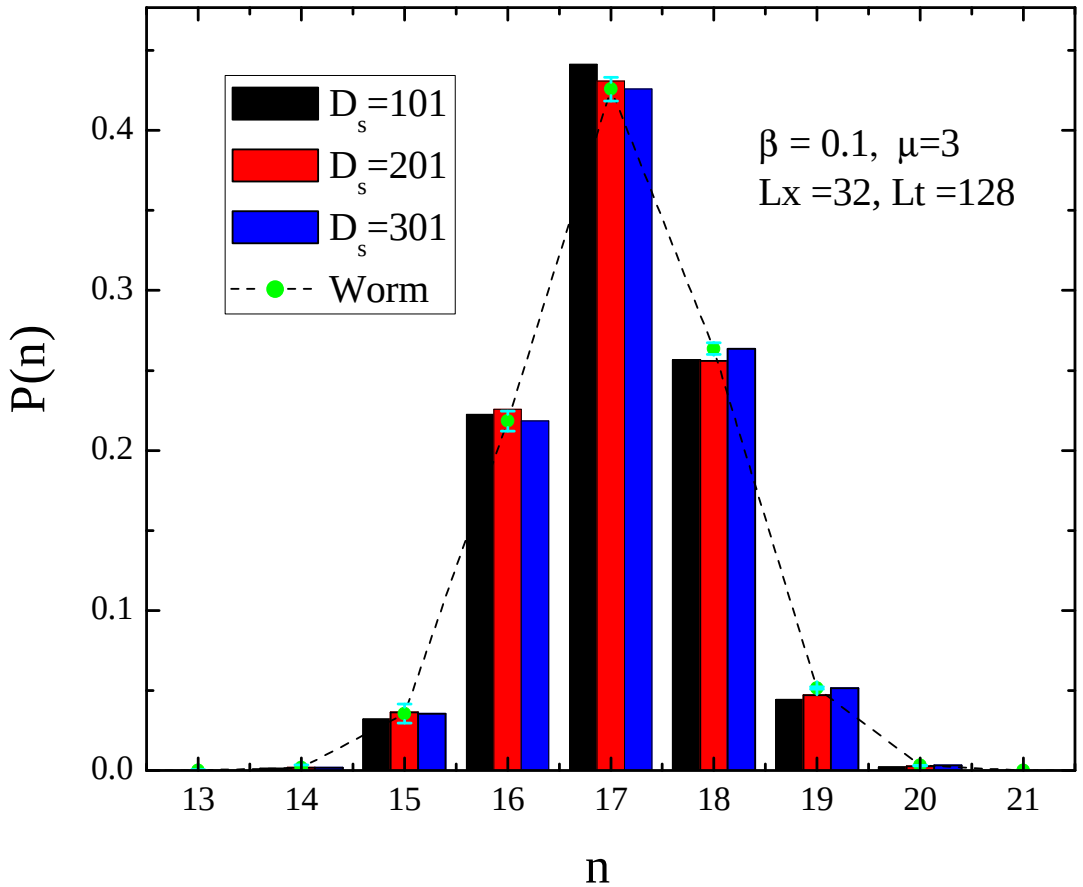

Figure: Comparison of the particle number distribution $P(n)$ from the worm algorithm and TRG with different D_s.

Entanglement entropy

We consider the subdivision of the system AB with density matrix $\hat{\rho}_{AB} \equiv \mathbb{T}^{L_t}/Z$ into two parts A and B (with equal spatial size). We define the reduced density matrix $\hat{\rho}_A$ as

$$\hat{\rho}_A \equiv \mathrm{Tr}_B \hat{\rho}_{AB}.$$

We define the entanglement entropy of A with respect to B as the von Neumann entropy of this reduced density matrix $\hat{\rho}_A$. The eigenvalue spectrum $\{\rho_{A_i}\}$ of the reduced density matrix can then be used to calculate the entanglement entropy

$$S_E = -\sum_i \rho_{A_i} \ln(\rho_{A_i}).$$

We use blocking methods until A and B are each reduced to a single site.

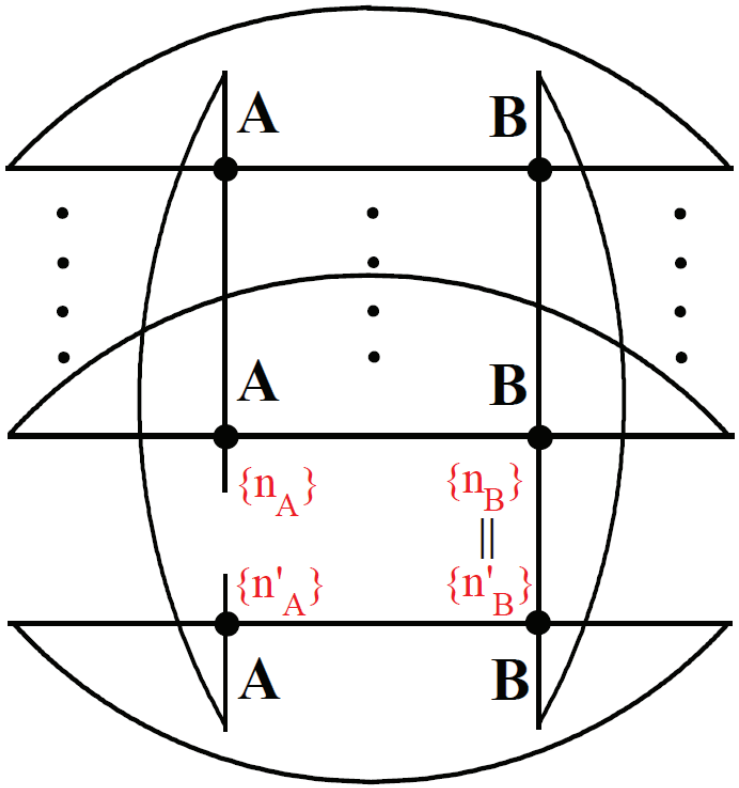

Figure: Illustration of the entanglement entropy calculation. The horizontal lines represent the traces on the space indices. There are L_t of them, the missing ones being represented by dots. The two vertical lines represent the traces over the blocked time indices in A and B.

Thermal entropy and entanglement entropy for $L_x = 4$

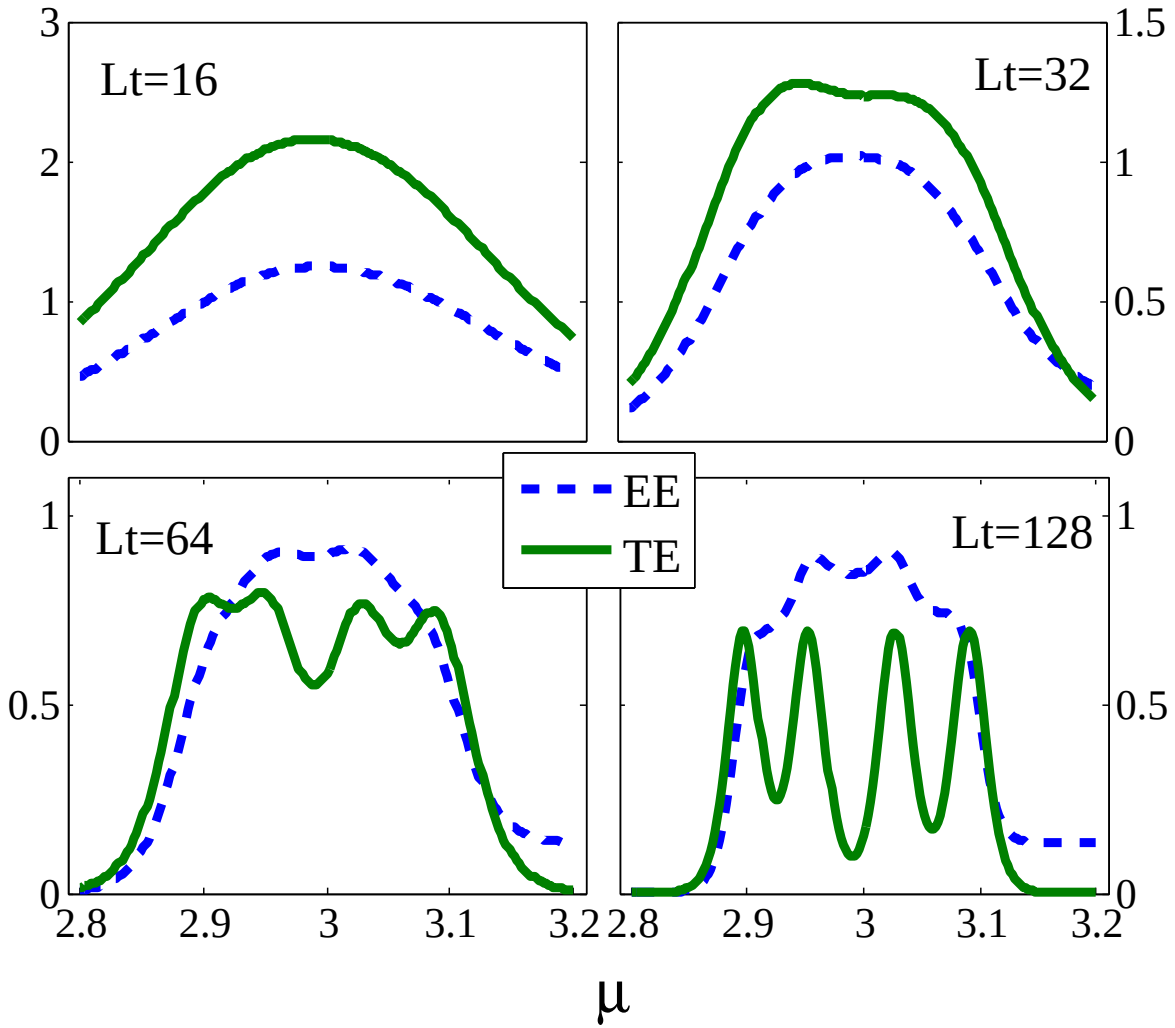

Figure: Entanglement entropy (EE, dash line) and thermal entropy (TE, solid line) for $\beta = 0.1$, $L_x = 4$ and $L_t = 16$, 32, 64 and 128.

Level crossings with increasing particle numbers

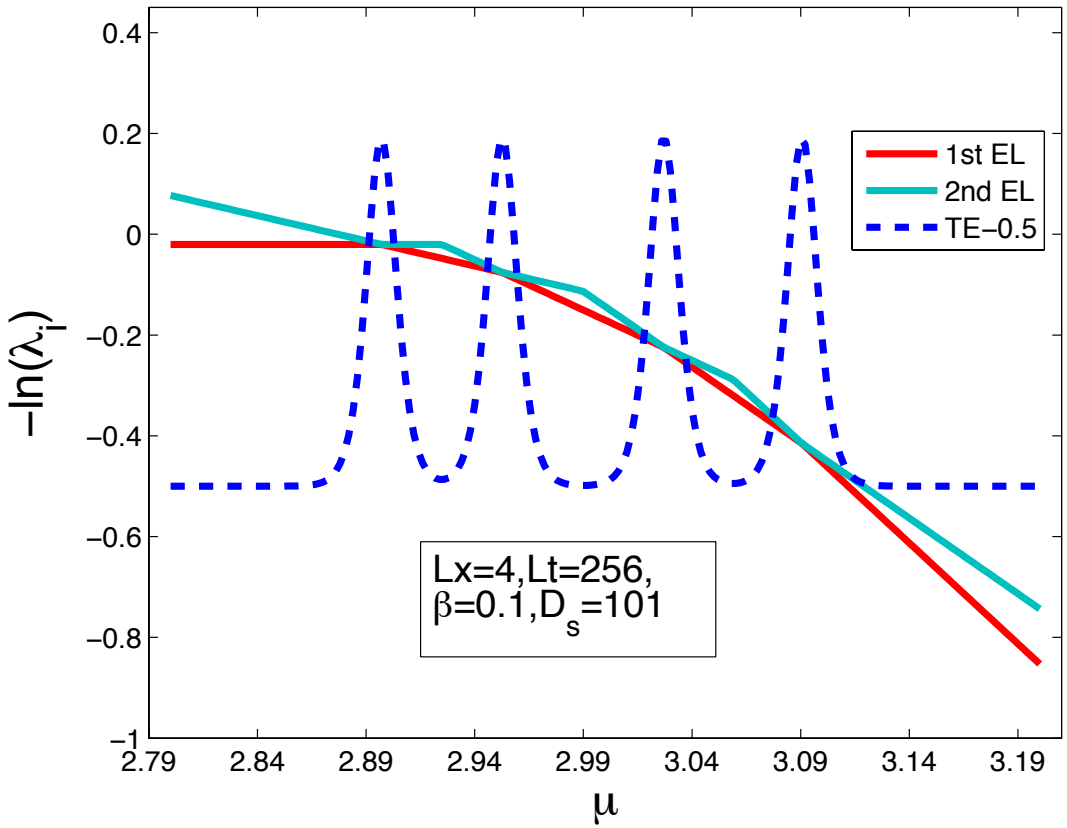

Figure: The two lowest energy levels (EL, $E_i = -\ln(\lambda_i)$) as a function of μ for $L_x = 4$, $L_t = 256$, $\beta = 0.1$. As μ increases, lines of successive slopes 0, -1, -2, -3, and -4 are at the lowest level. At each crossing, the thermal entropy jumps from 0 to $\ln 2$. The values of the thermal entropy are shifted vertically by -0.5 to make the figure readable.

Approximate spectroscopy for $L_x = 4$ (1507.01471)

Near $\mu = 2.90$, the lowest energy state changes from $|0000\rangle$ to

$$|\Omega, n = 1\rangle = \frac{1}{2}(|1000\rangle + |0100\rangle + |0010\rangle + |0001\rangle) \ .$$

The reduced density matrix for A = first two sites and B = last two sites in the limit where $L_t \to \infty$

$$\begin{aligned} \hat{\rho}_A &= \mathrm{Tr}_B \, |\Omega, n = 1\rangle \langle \Omega, n = 1| \\ &= \frac{1}{4}(|10\rangle + |01\rangle)(\langle 10| + \langle 01|) + \frac{1}{2} |00\rangle \langle 00| \ . \end{aligned}$$

A $n = 2$ state becomes the ground state near μ=2.95. It is in good approximation a linear superposition of the 6 states with two 0's and two 1's. The two states $|1010\rangle$ and $|0101\rangle$ have a slightly larger coefficient suggesting weak repulsive interactions. We also have contributions from states such as $|2000\rangle$ but with small coefficients.

Particle-hole symmetry

A $n = 3$ state becomes the ground state near μ=3.03.

$$|\Omega, n = 3\rangle = \frac{1}{2}(|0111\rangle + |1011\rangle + |1101\rangle + |1110\rangle) \ ,$$

which is $|\Omega, n = 1\rangle$ with 0's and 1's interchanged and one can interpret the 0 as "holes". Finally, near μ=3.10, $|1111\rangle$ becomes the ground states (with again many small corrections). In general, there is an approximate mirror symmetry about the "half-filling" situation.

For small β, the two state approximation (only 0 or 1 at the vertical lines at each site) is good (is it similar to a quantum XY model?)

Weakly interacting loops carrying a $n = 1$ current

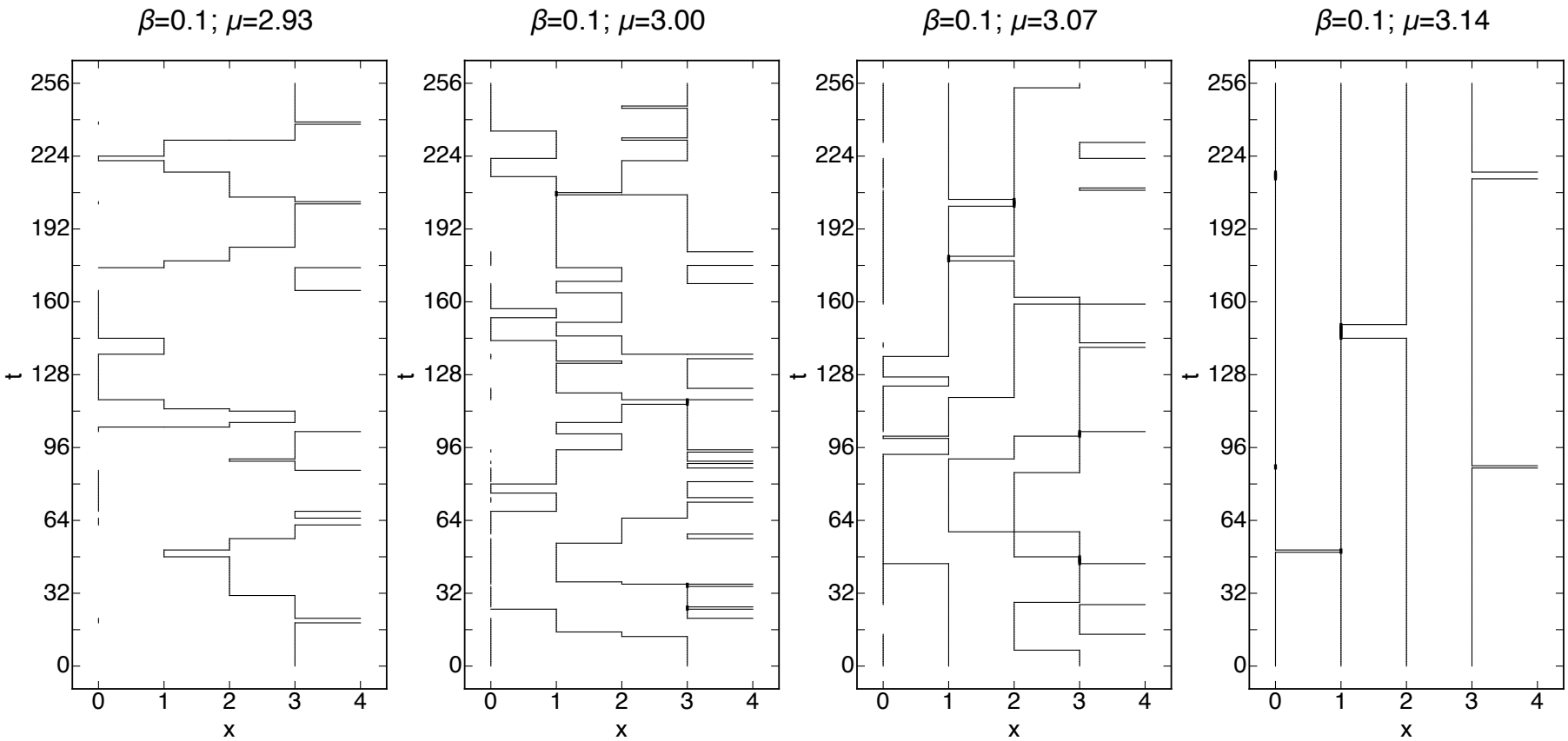

Figure: Worm configurations for μ =2.93 (n=1), 3.00 (n=2), 3.07 (n=3) and 3.14 (n=4) for $\beta = 0.1$, $L_x = 4$ and $L_t = 256$. Almost all the $|n|$' s are 0 or 1. Between most time slices we have n time links carrying a current 1 and $L_x - n$ time links carrying no current. In rare occasions, lines merge or cross. This illustrates the dominance of the states like $|1010\rangle$ over states like $|2000\rangle$.

The fine structure for $L_x = 4$, $L_t = 256$

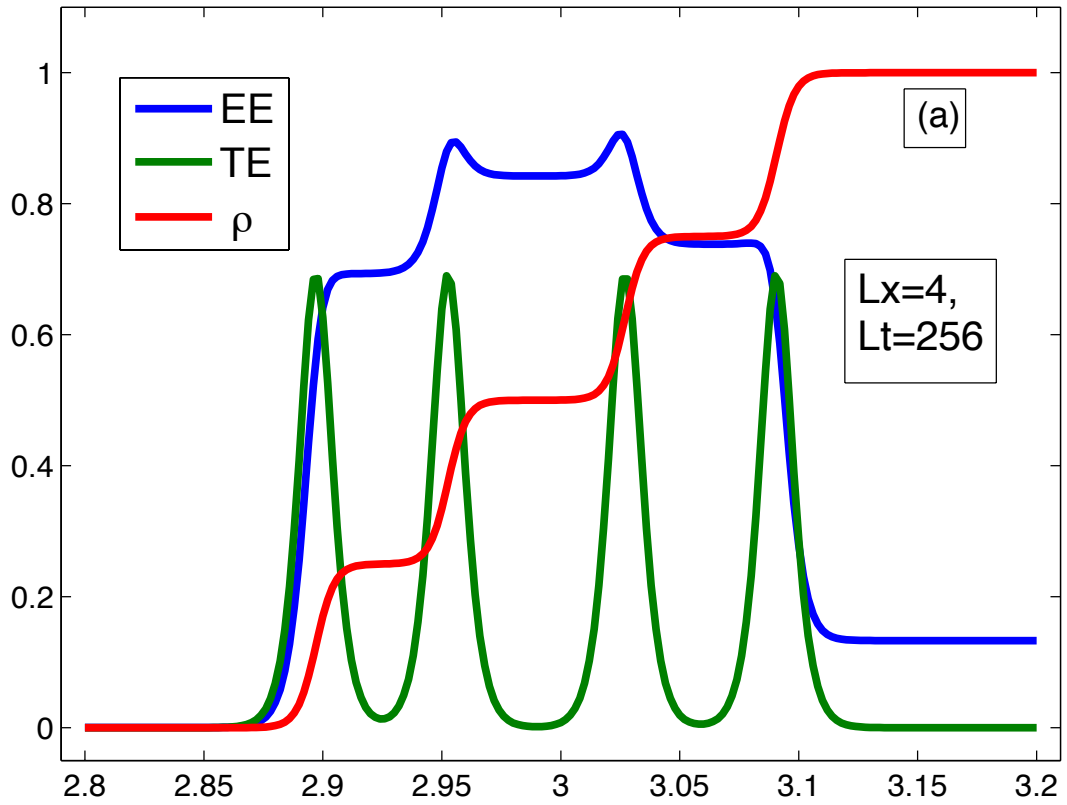

Figure: Entanglement entropy (EE, blue), thermal entropy (TE, green) and particle density ρ (red). The thermal entropy has $L_x = 4$ peaks culminating near $\ln 2 \simeq 0.69$; ρ goes from 0 to 1 in $L_x = 4$ steps and the entanglement entropy has an approximate mirror symmetry near half fillings where it peaks.

Similar features for $L_x = 16$ with $L_t = 1024$

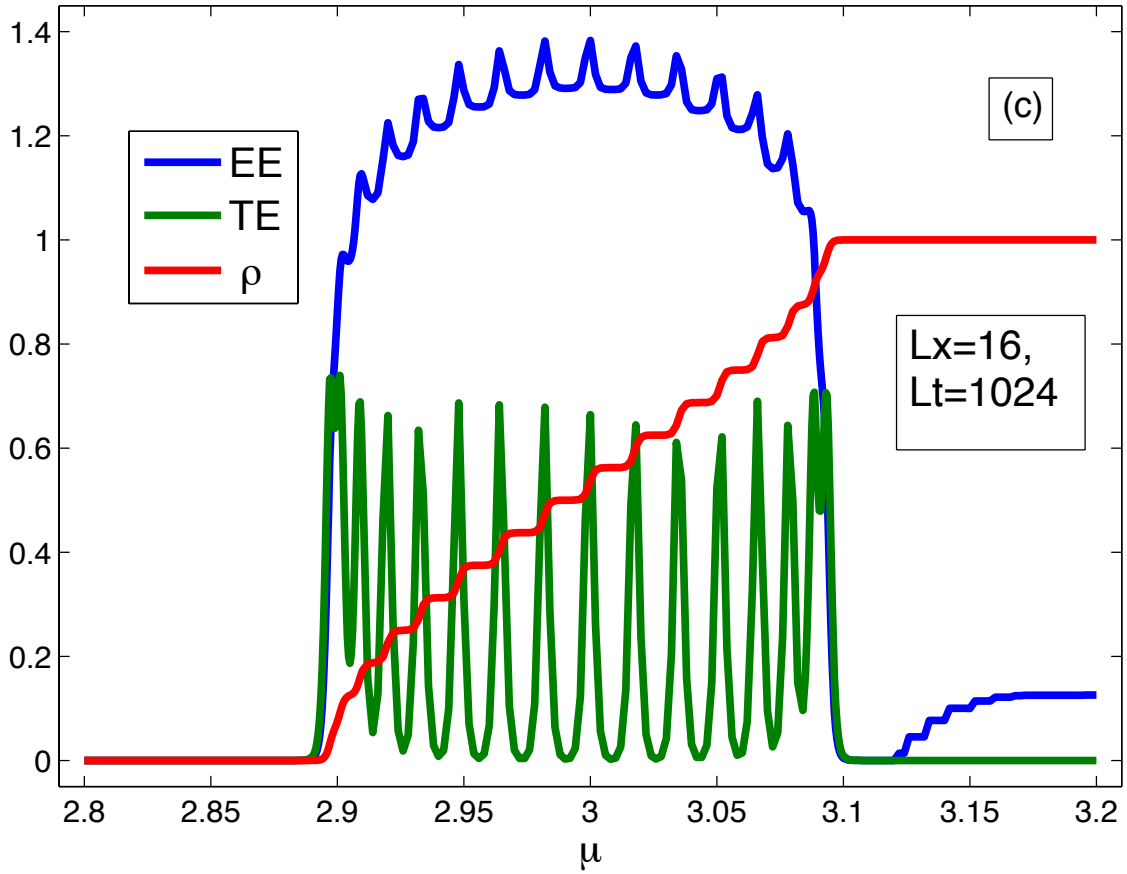

Figure: Entanglement entropy (EE, blue), thermal entropy (TE, green) and particle density ρ (red). The thermal entropy has $L_x = 16$ peaks culminating near $\ln 2 \simeq 0.69$; ρ goes from 0 to 1 in $L_x = 16$ steps and the entanglement entropy has an approximate mirror symmetry near half fillings where it peaks.

QCD with chemical potential on $S_1 \times S_3$

QCD at finite chemical potential in a small hyperspherical box Joyce C. Myers

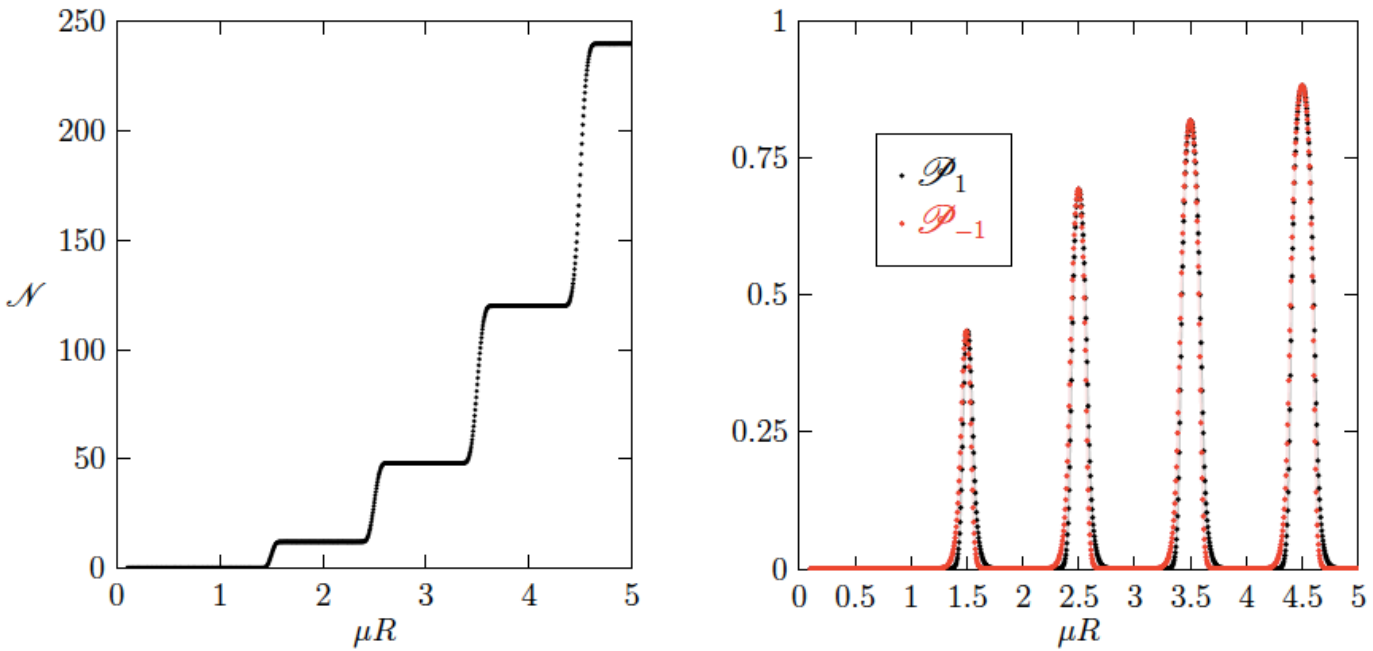

Figure 1: Quark number (Left) and Polyakov lines (Right) as a function of the chemical potential for QCD on $S^1 \times S^3$. (Right). $N = 3, N_f = 1, m = 0, \beta/R = 30$ (low T).

Figure: From: Simon Hands, Timothy J. Hollowood, Joyce C. Myers, arxiv 1012.0192, Lattice 2010.

Optimization through symmetry (Judah Unmuth-Yockey (Ph. D. 2016) and James Osborn)

- The particle number conservation allows a simplified parameterization of the tensor.
- For every tensor involved in contraction, one less sum/loop can be performed.
- In general, after one iteration, many states possess the same charge and a state can be labeled by its charge, and its degeneracy index.
- We can loop over the charges and treat the degeneracy index exactly as we treated the tensor indices in HOTRG (the unoptimized standard method).
- This gives good results when the number of charges has been reduced by iteration (near criticality).
- The initial iteration is delicate.

Initial Python benchmarks

- After the first couple iterations, the iteration time decreases drastically with the optimized method.
- After many iterations (infinite volume) additional iteration time is negligible.
- Computing time near the KT transition ($\beta = 1$, $\mu = 0$).

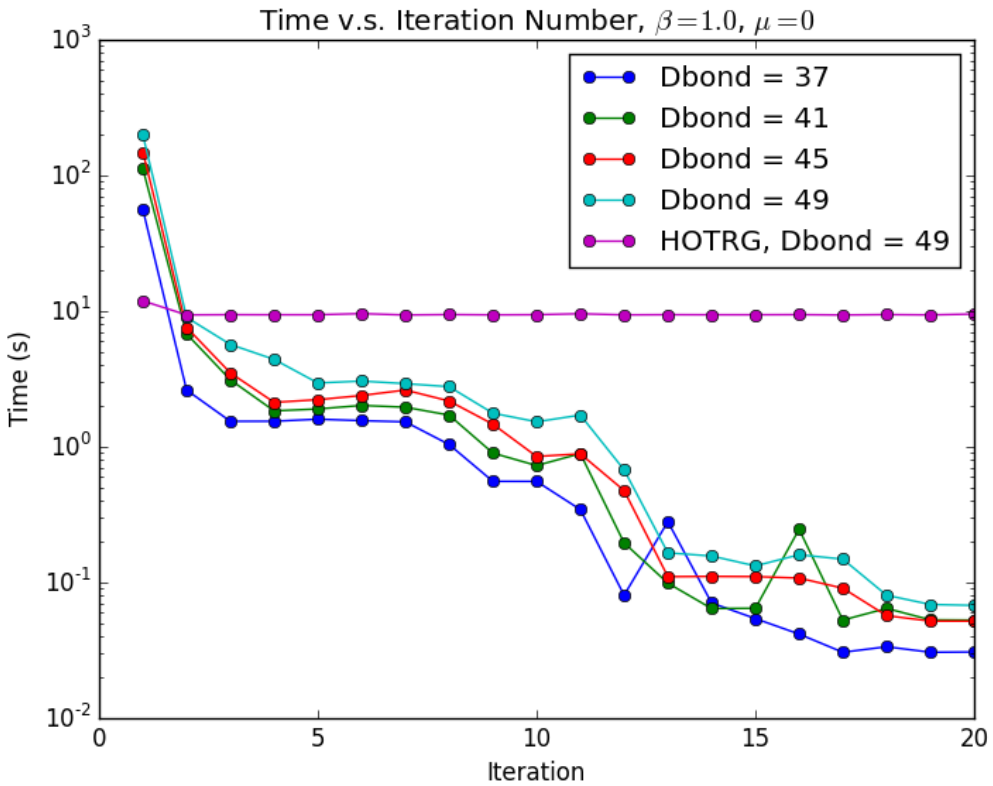

Initial Python benchmarks

- For a large enough number of states kept at each iteration (D_{bound}), the optimized method wins.

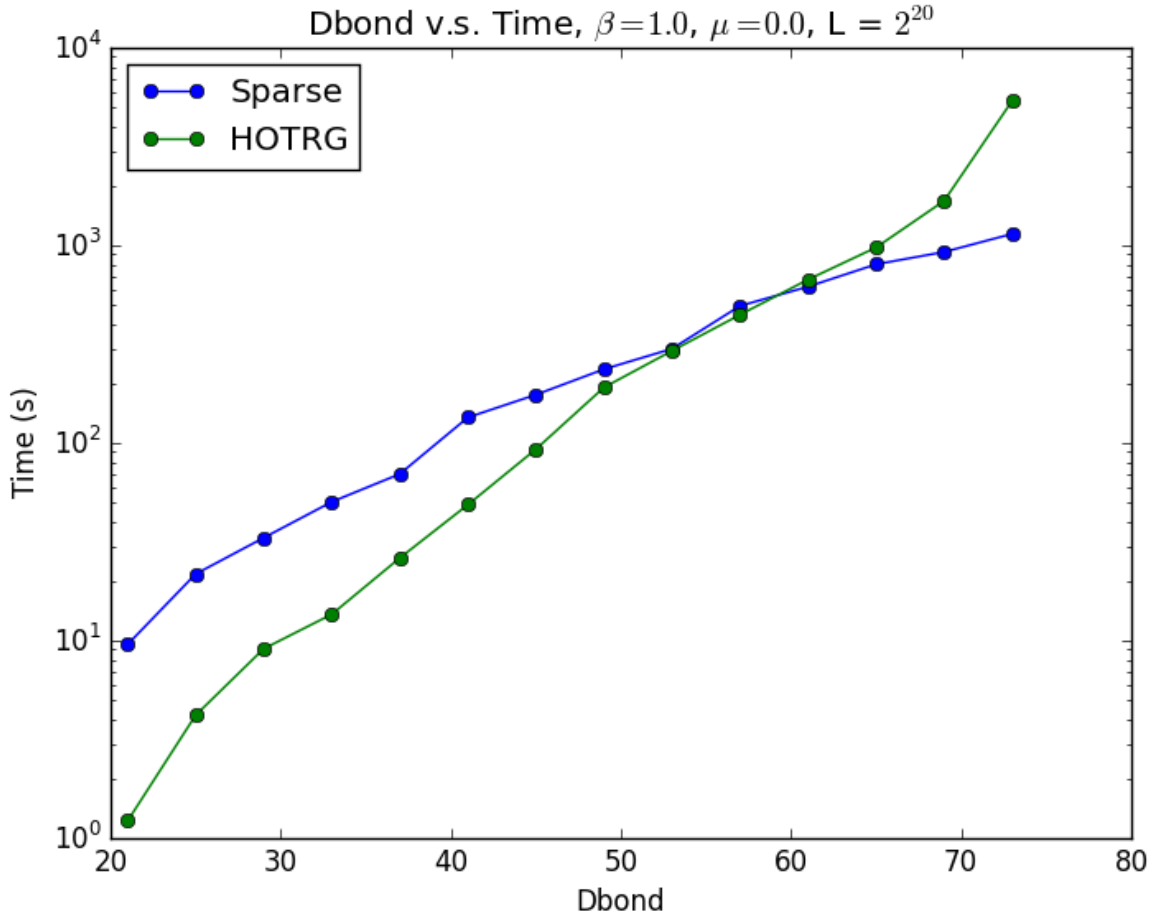

Conclusions

- The tensor renormalization group formulation allows reliable calculations of the particle density which can be checked with the worm algorithm.
- The TRG method can be used to calculate the thermal entropy and the entanglement entropy without using the replica trick.
- At sufficiently large L_t, the thermal entropy and the entanglement entropy show a rich fine structure as a function of the chemical potential.
- An approximate picture of weakly interacting loops winding one around the Euclidean time direction and carrying particle number one provides a particle-hole symmetry which justifies the mirror symmetry of the entanglement entropy with respect to half-filling.
- Particle number conservation allows more efficient TRG algorithms.

Thanks!!

Acknowledgments

This research was supported in part by the Department of Energy under Award Number DOE grant DE-SC0010114, and by the Army Research Office of the Department of Defense under Award Number W911NF-13-1-0119. This work utilized the Janus supercomputer, which is supported by the National Science Foundation (award number CNS-0821794) and the University of Colorado Boulder. The work was supported by the Natural Science Foundation of China for the Youth (Grants No.11304404). Judah Unmuth-Yockey was supported as Research Aid 206-LCF-1 by Argonne National Laboratory during Summer 2015.

Particle number distributions at different μ

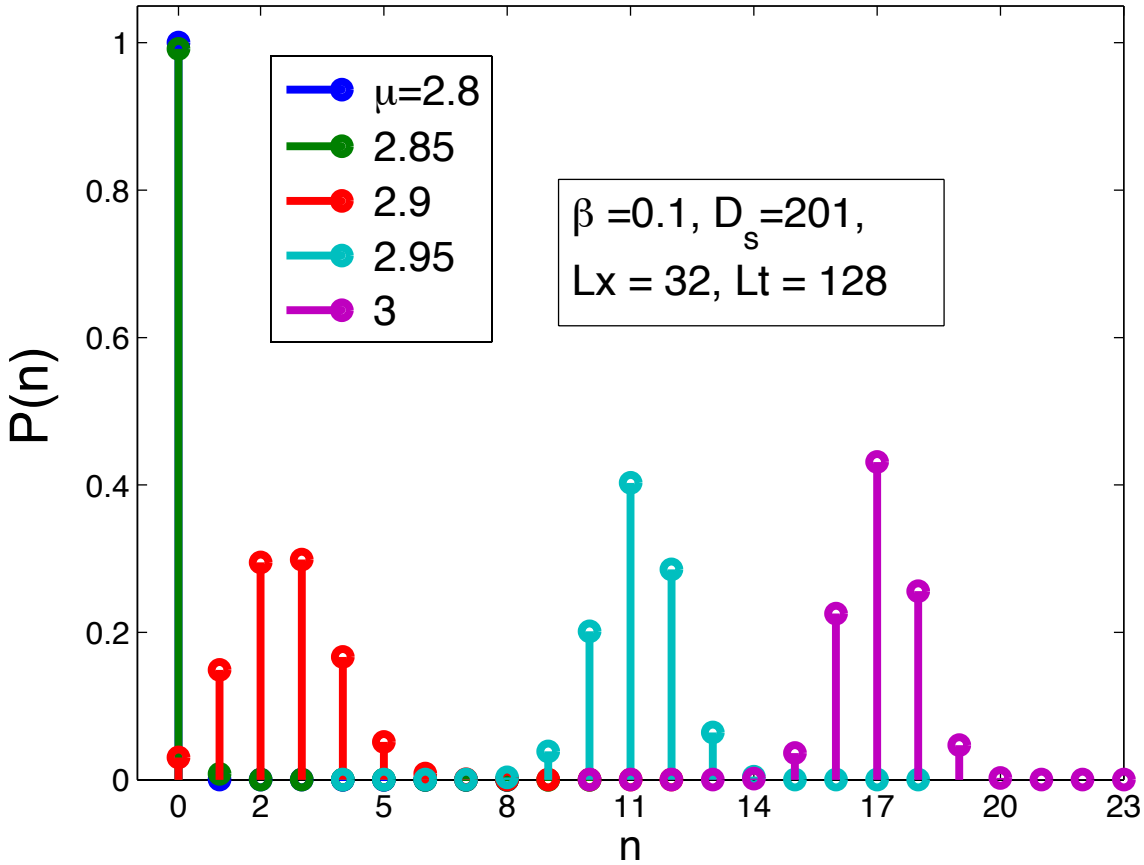

Figure: The particle number distribution $P(n)$ with μ taking different values at the boundary between the MI and SF phases. For $\mu = 2.80$ and 2.85, we only have $n = 0$. For $\mu = 2.90$, 2.95 and 3.0, there are three visible groups of bins. With μ increasing, the distribution shift to the right with larger most probable particle number.

Thermal entropy

We consider the system, denoted AB, and later subdivide it into two parts denoted A and B. The thermal density matrix $\hat{\rho}_{AB}$ for the whole system is

$$\hat{\rho}_{AB} \equiv \mathbb{T}^{L_t}/Z \ . \tag{1}$$

If the largest eigenvalue of the transfer matrix is non degenerate with an eigenstate denoted $|\Omega\rangle$, we have the pure state limit

$$\lim_{L_t \to \infty} \hat{\rho}_{AB} = |\Omega\rangle \langle\Omega|$$

We will work at finite L_t and will deal with the entanglement of thermal states. In general, the eigenvalue spectrum $\{\rho_{AB_i}\}$ of $\hat{\rho}_{AB}$ can then be used to define the thermal entropy

$$S_T = -\sum_i \rho_{AB_i} \ln(\rho_{AB_i}). \tag{2}$$

The fine structure of the SF phase ($L_x = 4$)

The fine structure of the SF phase between the MI phases can be approached by first considering the limit $\beta_{\hat{x}} = 0$ where the spacial sites decouple and the restoring $\beta_{\hat{x}} = \beta_{\hat{t}}$ perturbatively. The SF phases are approximately located near values of μ where $n^\star$ changes. To be specific, we will consider the example of $\beta = 0.1$, $L_x = 4$, where the transition occurs near $\mu_c = 2.997\cdots$ when $\beta_{\hat{x}} = 0$. In this limit, we have 16 degenerate states $|0,0,0,0\rangle$, $|1,0,0,0\rangle$, $\ldots$, $|1,1,1,1\rangle$ which can be organized in “bands" with $n = 0$ (1 state), $n = 1$ (4 states), etc. Below, we call the approximation where the indices inside the kets are only 0 or 1 the “two-state approximation".
The effect of $\beta_{\hat{x}}$ is to give these bands a width and lift the degeneracy. The energy levels are defined in terms of the eigenvalues of the transfer matrix as

$$E_i = -\ln(\lambda_i). \tag{3}$$